ADVANCED FUNCTIONAL MATERIALS
www.afm-journal.de

Coupled Ion-Gel Channel-Width Gating and Piezotronic Interface Gating in ZnO Nanowire Devices

Xixi Yang, Guofeng Hu, Guoyun Gao, Xuanyu Chen, Junlu Sun, Bensong Wan, Qian Zhang, Shanshan Qin, Wenliang Zhang, Caofeng Pan, Qijun Sun, and Zhong Lin Wang**

The piezotronic effect has been extensively investigated and applied to the third generation of semiconductors. However, there currently is no effective method compatible with microelectronics techniques to harness the piezotronic effect. In this work, a facile and low-energy-consuming method to couple the channel-width gating effect with piezotronic devices is developed by precisely patterning ion-gel electrolyte on ZnO NW. The ultrahigh capacitance of ion gel resulting from electrical double layers allows efficient modulation of the charge carrier density in ZnO NW at low gate voltage (2 V) to compensate for the piezotronic effect. The obtained output current variation under negative gate voltage (420%, i.e., enhanced piezotronic effect) is two times higher than that under zero or positive gate biases (200%). Through quantifying the reverse-biased Schottky barrier height and charge carrier density, it is found that the applied negative gate voltage depletes free electrons in ZnO NW and alleviates the screening effect on piezoelectric polarization charges, leading to enhanced piezotronic effect. Based on this, an ion-gel-gated piezotronic strain sensor is fabricated with enhanced gauge factor and tunable logic devices. It is believed that the coupled ion-gel and piezotronic gating effect is of great significance to the design of sophisticated and practical piezotronic devices.

1. Introduction

Piezotronic effect utilizes piezopotential to tune transport behaviors in semiconductor devices, which widely exists in noncentral symmetry wurtzite-structured nanomaterials (e.g., zinc oxide,[1,2] gallium nitride,[3] etc.) and odd-layered transition metal dichalcogenides (e.g., molybdenum disulfide[4]). By coupling of semiconducting and piezoelectric properties, the polarization charges induced by mechanical strain have great impact on the charge carrier transporting across the metal–semiconductor interface (or contact), giving rise to a strain-gated piezotronic transistor.[5] The piezotronic transistor inspired extensive research interests in piezotronic effect and relevant devices, such as piezotronic mechanosensors,[6] photodetectors,[7,8] chem/biosensors,[9,10] electromechanical switch,[11] memory,[12] etc. As the basic building block, piezotronic transistors are also integrated into piezotronic logic devices,[13,14] active tactile sensing matrix,[15] and high resolution light emitting diodes (LEDs) array,[16] exhibiting versatile and unprecedented characteristics. To availably utilize piezotronic effect, the influence of chemical doping, band structure engineering, and even external environment conditions (e.g., temperature,[17] humidity,[18] and external electric field[19]) on the piezotronic devices has been intensively investigated. However, the studied chemical engineering and environment conditions are not compatible with microelectronics technology, lack of efficient way to integration with current piezotronic devices. Hence, a simple, controllable, safe, and low-power-consuming way to harness piezotronic effect is urgent to be developed.

Ionic liquid, a polar binary salt in liquid state, is a nonvolatile, nontoxic, and highly thermal/chemical stable electrolyte. With wide electrochemical window, it promises to be applicable

X. Yang, G. Hu, G. Gao, X. Chen, J. Sun, B. Wan, Q. Zhang, S. Qin, W. Zhang, Prof. C. Pan, Prof. Q. Sun, Prof. Z. L. Wang
Beijing Institute of Nanoenergy and Nanosystems
Chinese Academy of Sciences
Beijing 100083, P. R. China
E-mail: sunqijun@binn.cas.cn; zhong.wang@mse.gatech.edu
X. Yang, G. Hu, G. Gao, X. Chen, J. Sun, B. Wan, Q. Zhang, S. Qin, W. Zhang, Prof. Q. Sun, Prof. Z. L. Wang
School of Nanoscience and Technology
University of Chinese Academy of Sciences
Beijing 100049, P. R. China
The ORCID identification number(s) for the author(s) of this article can be found under https://doi.org/10.1002/adfm.201807837.
X. Yang, G. Gao, X. Chen, Q. Zhang
CAS Center for Excellence in Nanoscience
National Center for Nanoscience and Technology (NCNST)
Beijing 100190, P. R. China
Prof. Q. Sun, Prof. Z. L. Wang
Center on Nanoenergy Research
School of Physical Science and Technology
Guangxi University
Nanning 530004, China
Prof. Z. L. Wang
School of Materials Science and Engineering
Georgia Institute of Technology
Atlanta, GA 30332-0245, USA

DOI: 10.1002/adfm.201807837

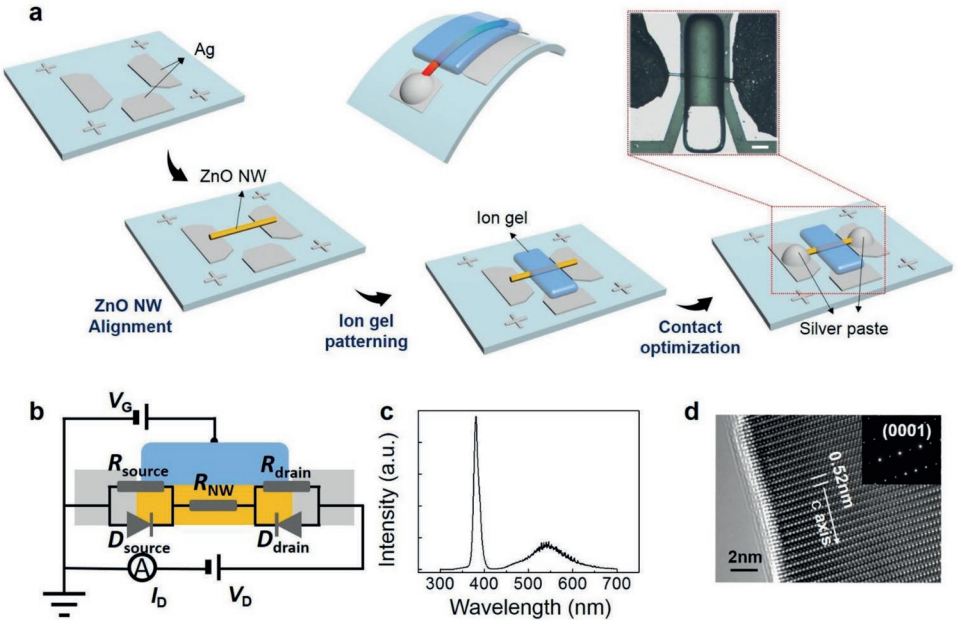

Figure 1. a) Schematic illustration of the ZnO piezotronic device fabrication process. The inset is an optical microscopy image of the device, the scale bar is 100 µm. b) Equivalent circuit diagram of the device. c) The PL spectrum of ZnO NWs. d) HRTEM image of the ZnO NWs and the corresponding SAED pattern.

in various electrochemical and electronic devices, such as batteries,[20] supercapacitors,[21] electrochromic devices,[22] actuators,[23] etc. When an ionic liquid is interfaced with solid under electric field, the ions migrate to the liquid/solid interface and accumulate compensated charges to form an electrical double layer (EDL), which can act as a nanogap capacitor to create an ultrahigh electric field at the interface. Particularly, the ultrahigh electric field promotes ionic liquid to be comprehensively used as the gate dielectrics for high performance field effect transistor.[24,25] Similarly, the EDL induced interface electric field is applicable to piezotronic transistor to efficiently modulate the piezotronic effect in much lower voltage compared with the external high electric field modulation.[19] To achieve practical solid-state piezotronic devices modulated by ionic liquid, demanded polymer networks (e.g., di/triblock copolymer, UV-cross-linked polymer, etc.) can be swollen in ionic liquid gel to overcome the liquid-state drawback. The achieved ion-gel is also required to have excellent mechanical properties without sacrifice of ionic mobility.

In this work, we developed a facile and low-energy-consuming way to coupling ion-gel-gating (i.e., channel-width gating) and piezotronic effect (i.e., interface gating) by precisely patterning ion-gel electrolyte on zinc oxide nanowire (ZnO NW). The formed EDL with ultrahigh capacitance during ion-gel-gating allowed efficient modulation on the charge carrier density in ZnO NW at low voltage (≤2 V). The obtained output current variation under negative gate voltage (420%) was more than two times higher than that under zero or positive gate biases (200%). To explore the underlying modulation mechanism, the ion-gel-gated piezotronic device was modeled as two back-to-back Schottky diodes connected via a variable resistor (metal–semiconductor–metal (M–S–M) model), figured out with thermionic field emission theory. The Schottky barrier variation at a strain of 0.96% was increased from 0.09 to 0.18 eV when the applied gate bias changed from 2 V to –2 V, indicating an enhanced piezotronic effect under negative gate bias. The modeling results certified that the applied negative gate voltage could deplete the free electrons in ZnO NW (i.e., increase the channel-width) and alleviate its screening effect on piezoelectric polarization charges, leading to enhanced piezotronic effect. This mechanism was further interpreted vividly with energy band diagrams. Based on this, we fabricated solid-state ion-gel-gated ZnO NW piezotronic strain sensor with enhanced gauge factor (over 400) and tunable piezotronic logic devices. We believe the ion-gel-gated piezotronic effect is of great significance to provide guidance for the design of sophisticated and practical piezotronic device arrays.

2. Results and Discussion

Figure 1a illustrates the fabrication process of the ion-gel-gated ZnO NW piezotronic device. Ag pads for gate, source–drain electrodes, and aligner marks were patterned on polyethyleneterephthalate (PET) substrate (1 cm × 3 cm, 500 µm thick) by standard lift-off process. The ultralong ZnO NWs used in this work were synthesized via a vapor–liquid–solid growth method by chemical vapor deposition (CVD),[26] through which the ZnO NWs grew along the preferential direction to minimize the surface free energy. The diameters of the grown ZnO NWs were around 0.5–5 µm and the lengths were 50–1000 µm. The demanded ZnO NWs (piezotronic fine wires (PFWs)[6]) were picked out and located between the source and drain electrodes, creating a M–S–M structure. Next, photocurable ion-gel (a mixture of 1-ethyl-3-methylimidazolium bis(trifluoromethylsulfonyl)imide ion liquid, 2-hydroxy-2-methylpropiophenone photoinitiator, and poly(ethylene glycol) diacrylate cross-linker in the weight ratio of 90:2:8) was

precisely patterned across the ZnO NWs and a portion of the gate electrode. Finally, silver paste was dropped on two ends of the ZnO NW to form fully enclosed electrodes. It helped to realize good electrical contact and distributed the piezoelectric polarization charges at two ends of the ZnO NW to maximize the piezotronic behaviors (Figure S1, Supporting Information). Inset of Figure 1a shows the optical image of the ion-gel-gated ZnO NW piezotronic device (channel length is 300 μm). The equivalent circuit diagram is shown in Figure 1b. ZnO NW located between two Ag electrodes in M–S–M structure is considered as two back-to-back Schottky diodes in series connection with a variable resistor (R_{NW}). Ion-gel covered on ZnO NW is a solid-state electrolyte gate dielectric, in which the formation of electrical double layer can lead to ultrahigh capacitance for efficient gating modulation of the charge carriers in ZnO NW. In the ion-gel-gated ZnO NW piezotronic device, the piezopotential induced by piezoelectric polarization charges under external strain can be considered as the first "gate" to modulate the charge transport across ZnO NW, i.e., piezotronic effect. Applied voltage on the patterned ion-gel can be considered as the second "gate" to modulate the piezotronic effect, i.e., enhancing/weakening the screening effect of polarization charges by modulating the free electrons in ZnO NW (the working mechanism will be discussed below in details). We selected the ion-gel to modulate the piezotronic effect of ZnO NW for three reasons: i) ion liquid gelation with photocurable polymer promised the precise patterning on piezotronic ZnO NW device; ii) the formation of EDLs led to ultrahigh capacitance for low voltage and efficient modulation; iii) excellent flexibility and mechanical properties of ion-gel insured the persistent and conformal contact with ZnO NW to realize continuous gate bias imposition. This was the first time to utilize solid-state electrolyte (ion-gel) to modulate the piezotronic effect, which provided an efficient and in situ way to fabricate compact tunable piezotronic devices. Notably, to investigate the piezotronic effect in ZnO NW, we had to sacrifice its high electron mobility to weaken the screening effect of free electrons on piezoelectric polarization charges. This was also the reason to the selection of PFWs. Therefore, we mainly focused on the ion-gel-gating modulation of the charge density for the screening effect other than the transport properties.

The optical and crystal properties of the synthesized ZnO NW were characterized by photoluminescence (PL) spectrum and high-resolution transmission electron microscopy (HRTEM), respectively. The PL spectrum (Figure 1c) presents a sharp and intensive near-band-edge emission peak centered at about 380.6 nm and a broad and weak green emission band (associated with ionized oxygen vacancy defects in ZnO NW), demonstrating a favorable single-crystalline structure of the ZnO NWs.[27] To further verify the high crystal quality of ZnO NWs, HRTEM and the corresponding selected area electron diffraction (SAED) pattern were conducted to the ZnO NW samples. As shown in Figure 1d, the distance between the adjacent lattice planes is 0.52 nm, in good agreement with the *c*-axis lattice constant of hexagonal ZnO. It indicated the ZnO NWs were single crystalline and the growth direction was along the *c*-axis ([0001]).[28]

To get insight into the ion-gel-gating modulation on charge carrier density in ZnO NW, **Figure 2**a illustrates the relevant

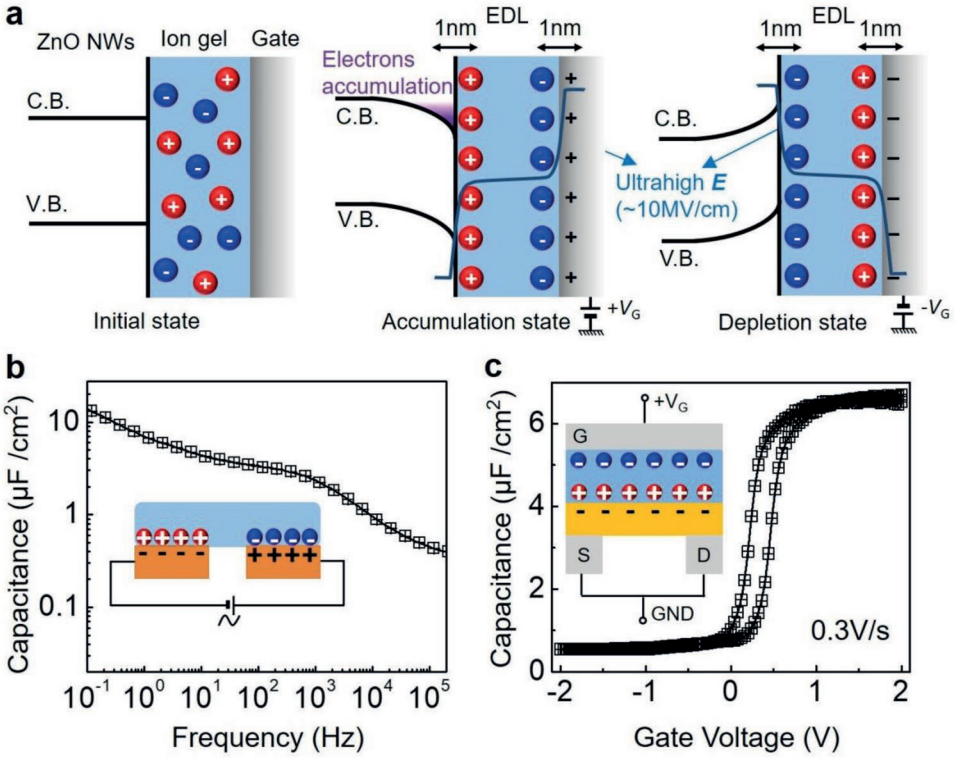

Figure 2. a) Schematic of the influence of EDL on the energy band structure of ZnO under different gate voltages (V_G = 0 V, V_G = 2 V, and V_G = –2 V), and the potential drop in two EDLs as well as ion-gel bulk was sketched with dark blue lines. b) Capacitance versus frequency for a capacitor based on ion-gel in this work. c) Capacitance versus gate voltage based on ion-gel gated ZnO NW device in this work.

energy band diagrams under different gate voltages (V_Gs). At the initial state without applying V_G (V_G = 0 V, left panel in Figure 2a), cations and anions were distributed randomly in ion-gel. The energy band of ZnO NWs was flat (flat band state). When a positive V_G was applied to the ZnO NW through ion-gel (V_G = 2 V, middle panel in Figure 2a), the anions were attracted to the interface of gate/ion-gel interface to form an EDL (≈1 nm) due to the electronic insulating properties of ion-gel. Meanwhile, the cations migrated to the ion-gel/ZnO interface and caused the accumulation of electrons in ZnO NW (accumulation state). The accumulated electrons resulted in the downward bending of the energy band in ZnO NWs and enhanced the transport properties. When the negative V_G was applied (V_G = −2 V, right panel in Figure 2a), the cations were attracted to the interface between gate electrode and ion-gel, while the anions were repelled to the opposite side and depleted the electrons in ZnO NW. This behavior led to upward bending of the energy band in ZnO and suppressed the output currents. Notably, the formed EDLs consisting of electrons (or holes), the compensated cations (or anions), and adsorbed solvent molecules could be regarded as two nanogap capacitors (thickness ≈1 nm),[29] in which the electric potential dropped in an exponential function (Figure S2a, Supporting Information) and the potential drop in ion-gel bulk was negligible. Therefore, the applied gate voltage at 2 V could be simply separated into two potential drops at gate/ion-gel interface and ion-gel/ZnO interface, respectively. In order to figure out the effective potential drop at ion-gel/ZnO interface, which had a direct electrostatic control on the charge carrier density in ZnO NW, a reference electrode (a thin gold wire) was inserted in the ionic gel between the gate electrode and the ZnO NW channel (Figure S2c, Supporting Information). The effective potential drop (i.e., the reference voltage, V_R) was measured between the reference electrode and source electrode.[30,31] The correlation of V_R and the applied V_G is shown in Figure S2d (Supporting Information). The effective potential drop was evaluated to be ≈1.75 V, which could still induce an ultrahigh electric field (≈17.5 MV cm^{-1}) across the ion-gel/ZnO interface, resulting in a strong electrostatic control on the charge carrier density in ZnO NW for subsequent modulation of piezotronic effect that occurred at the two end surfaces of the ZnO nanowire.

Electrochemical impedance spectroscopy was conducted to characterize the capacitive behaviors of ion-gel during ions migration and EDL formation process. A planar metal–insulator–metal structure was used to analyze the capacitance variation (inset of Figure 2b). The distance between the two Au electrodes was 50 µm. And the ion-gel was patterned across a portion of each electrode. The equivalent circuit diagram of the ion-gel dielectric could be simplified as a series connection of three resistor-capacitor circuits under AC voltage in different frequencies (two represent EDLs, and one indicates ion-gel bulk phase, Figure S2b, Supporting Information). Figure 2b exhibits the ion-gel capacitance (C) versus the frequency (f) of applied voltage, defined by $C = -1/2\pi f Z''$ (Z'' is the imaginary impedance[32,33]). The ion-gel capacitance was over 10 µF cm^{-2} at a low frequency of 0.1 Hz and still higher than 1 µF cm^{-2} at 10^4 Hz, indicating that the gelation polymer network did not inhibit the migration speed of the ions (i.e., ionic mobility). The corresponding phase angle versus AC voltage frequency is shown in Figure S3a (Supporting Information). To precisely describe the capacitive behavior of the ion-gel all-round ZnO NW, we further conducted the capacitance characterization through a displacement current measurement method.[34,35] In this method, the source and drain electrodes were connected to ground and the gate voltage was swept at a fixed rate (inset of Figure 2c). The measured displacement current (I_{disp}) is shown in Figure S3b (Supporting Information). The V_G dependent capacitance can be extracted from $I_{disp} = AC\frac{dV_G}{dt}$, where C is the specific capacitance of ion-gel, A is the channel area (≈500 µm^2), and $\frac{dV_G}{dt}$ is the sweep rate (0.3 V s^{-1}), respectively. As shown in Figure 2c, the EDL capacitance of ion-gel increased from 1.0 to 6.5 µF cm^{-2} with V_G changed from 0 to 2 V. The increased capacitance of ion-gel according to applied different V_Gs could be attributed to two reasons: i) the accumulation of more ions at the ion-gel/ZnO interface; ii) the Fermi level of ZnO NW moving toward the conduction band.

To characterize the coupling of ion-gel gating and piezotronic effect in ZnO NW, over 40 ZnO NW devices were selected with good piezoelectric properties and tested. Over 100 times of electrical annealing process were conducted to the selected ZnO NW devices to achieve the stable output performance. A numerical control microdisplacement stage was utilized to precisely apply the external strains to the ZnO NW piezotronic devices (Figure S4a, Supporting Information). As the thickness of the PET substrate (500 µm) was much larger than the diameter of the ZnO NWs (5 µm), the strain applied on the substrate could be regarded as a uniform strain applied in the longitudinal direction of the ZnO NW. The stain in the longitudinal direction (ε) was estimated as $\varepsilon = d/2R$ (Figure S4b, Supporting Information), where d was the thickness of the PET substrate and R was the equivalent bending radius.[36,37] **Figure 3** shows the electrical performance of ZnO NW device under applied strains and gate voltages. Two obvious transport properties of the ZnO NW were observed: 1) The nonlinear current–voltage (I–V) characteristics (rectifying behaviors) indicated the Schottky barriers formed between ZnO NW and silver electrodes, which was a typical feature of piezotronic fine wires (i.e., Schottky contacts at its two metal ends but with distinctly different barrier heights). This was preferential for highly sensitive Schottky-barrier dominated strain sensor. 2) Asymmetry output currents in opposite drain voltages (V_Ds) revealed that the piezotronic effect dominated the transport behaviors in the ZnO NW devices other than piezoresistive effect, which commonly existed in many semiconducting materials and showed symmetrical output performance under opposite V_Ds. The typical nonlinear and asymmetry I–V curves also represented that the ions in ion-gel are in electrostatic (or van der Waals) interaction with ZnO NW, which did not induce redundant chemical doping (or chemical bonding) to affect the piezotronic effect. The asymmetry output performance (typical piezotronic effect) was attributed to the fact that opposite polarization charges were generated at either end of ZnO NW under external longitudinal strains. The M–S contact with negative polarization charges accumulated exhibited an increased Schottky barrier height (SBH) to electrons transport (majority charge carriers in ZnO NW), while the other contact exhibited decreased SBH. The opposite variations of SBH would result in the asymmetry trends of output currents under positive/negative V_Ds. The

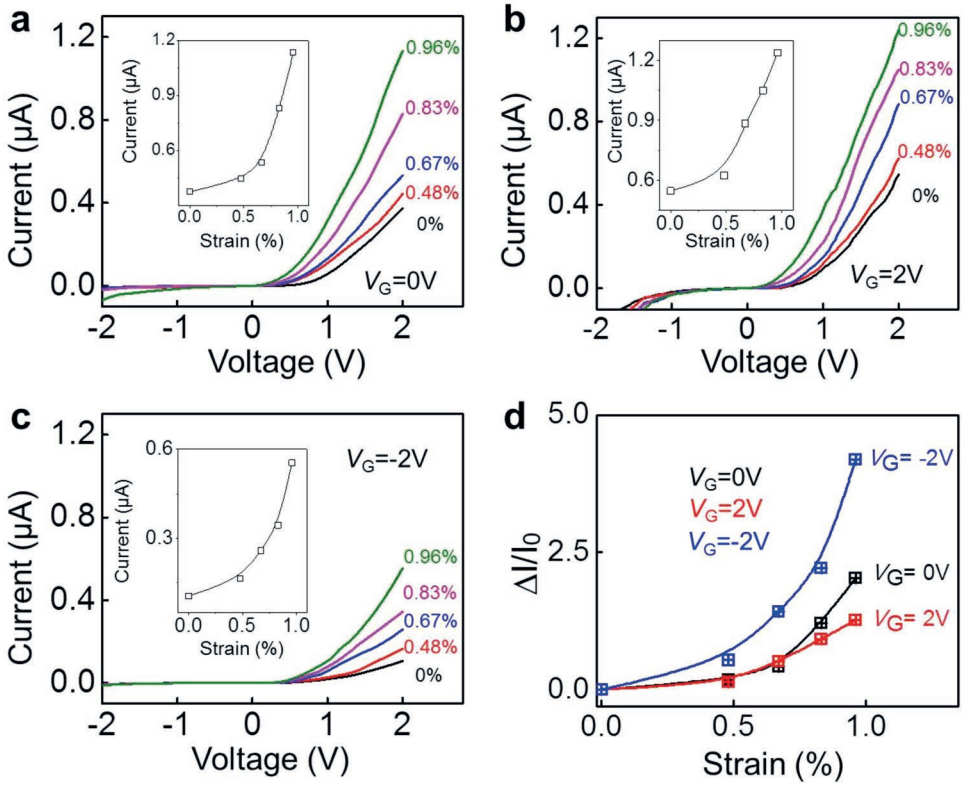

Figure 3. Transport behavior of the device gated by ion-gel with a) $V_G = 0$ V, b) $V_G = 2$ V, and c) $V_G = -2$ V under applied strains. Insets are the corresponding curves of output currents versus strains with $V_D = 2$ V. d) Relative changes of the current under different applied strains and V_Gs with $V_D = 2$ V.

corresponding enlarged image of transport behavior in negative V_D range was shown in Figure S5a–c (Supporting Information). No obvious variation trends were observed, which might be attributed to the competition between piezoresistive effect (band structure change) and piezotronic effect (Schottky barrier change).

As the gating modulation was independent of V_D directions, only the electrical transport behaviors under positive V_D were analyzed in the following discussion. As shown in Figure 3a, when the strain was increased from 0% to 0.96%, the output current was increased from 0.37 to 1.13 μA at $V_D = 2$ V without any gate bias. Output properties of the ZnO NW device under external gate bias are shown in Figure 3b,c. As electrons were the major carriers in n-type ZnO in this work, positive V_G accumulated the electrons in ZnO NW, resulting in higher output current under applied strain at 0.96% (1.24 μA at $V_D = 2$ V, inset of Figure 3b) compared with the output currents without gate bias (1.13 μA at $V_D = 2$ V, inset of Figure 3a). By contrast, negative V_G led to overall decrement of the output current due to the depletion of electrons in ZnO NW. A control sample with ZnO NW transferred on silicon wafer was characterized to compare with ion-gel-gated device (Figure S6, Supporting Information). To achieve an output current of 0.45 μA under the same V_D at 2 V, the gate bias required for SiO_2/Si substrate was 40 V, 20 times higher than the required gate bias for ion-gel-gated device (2 V). This is a factual proof that ion-gel-gating is promising for low voltage modulation.

Generally, the effective Schottky barrier height is one of the main physical parameters to describe the device transport properties with rectifying characteristic, especially the transport across the contact. In this work, we are more interested in the SBH change under certain fixed strains, which is a good quantitative evaluation of the piezotronic effect and clarifies how the external factors affect piezotronic behavior. To evaluate the ion-gel-gating modulation on the transport properties of the piezotronic device, we extracted the relative change of currents ($(I_\varepsilon - I_0)/I_0$) versus applied strains under different V_Gs (2, 0, and −2 V), as shown in Figure 3d. All the current variations increased with the increased external strains. However, the current variation with ion-gel-gating voltage at −2 V was 420% under a strain of 0.96%, two times larger than the current variation with zero gate bias (200%). Under the positive gating voltage at 2 V, the current variation was lowest (127%). The enhanced current variation under negative V_G was attributed to the enhanced piezotronic effect, i.e., negative V_G depleted the electrons in ZnO NW (or increased the channel width) and alleviated its screening effect on positive polarization charges at the source-electrode/ZnO interface,[38] which dominated the transport properties of the piezotronic device.

To quantitatively elaborate the proposed mechanism, we simulated the transport properties of our device through M–S–M model to extract the related device parameters. Generally, the M–S–M model is premised on the basis of the following two points[39]: i) the radius of the 1D semiconductor should be larger than the electron de Broglie wavelength (a few to tens nm), so that quantum confinement can be ignored and the effective mass estimation of the carrier is valid; ii) the total

length of the semiconductor should be longer than the depletion length (<220 nm) associated with the two Schottky barrier, so the undepleted part can be described by a constant resistor and approximated using the Ohmic law. In this work, the radiuses of the selected ZnO NWs were from ≈100 nm to 10 µm and the lengths are ≈1 mm, both of which satisfied the assumptions above. In the M–S–M model, the device structure was simulated as a resistor sandwiched between two back-to-back Schottky barriers, as shown in Figure 1b. The applied V_D distributions (on the undepleted ZnO NW and two Schottky barriers) and current density crossing the whole device were necessary to be obtained by solving the corresponding *I–V* relationships with a well-developed Matlab GUI program (PKUMSM).[40] By fitting the experimental and theoretical curves, related parameters (including the effective heights of the two Schottky barriers, carrier density, carrier mobility, undepleted ZnO NW conductance, etc.) were achieved. One of the example fitting curves (ε = 0.83%, V_G = −2 V) is shown in Figure S7a (Supporting Information). The calculated carrier density in ZnO NW is shown in **Figure 4**a, increasing from 0.85 × 10^{18} cm^{-3} to 1.78 × 10^{18} cm^{-3} with V_G increasing from −2 to 2 V.

In the piezotronic device, the *I–V* characteristic is mainly determined by the reverse-biased Schottky barrier (ϕ_b), which can be extracted from the thermionic field emission theory

$$J = -\frac{A^{*}T\left(\pi q E_{00}\right)^{\frac{1}{2}}}{\kappa} \times \exp\left(-\frac{\phi_b}{qE_0}\right)\left[q\left(V-\xi\right)+\frac{\phi_b}{\cosh^2\left(qE_{00}/\kappa T\right)}\right]^{\frac{1}{2}} \times \exp\left[V_D\left(\frac{q}{\kappa T}-\frac{1}{E_0}\right)\right] \quad (1)$$

where J is the current density flowing through the reverse-biased Schottky barrier, A^* is the Richardson constant of the ZnO NW, ξ is the distance between the bottom of the conduction band and the Fermi level, and $E_0 = E_{00}\coth\left(\frac{qE_{00}}{\kappa T}\right)$ with $E_{00} = \frac{\hbar}{2}\left[\frac{N_d}{m_n^{*}\varepsilon_S\varepsilon_0}\right]^{\frac{1}{2}}$. Thereinto, N_d is the doping density, m_n^{*} is the effective mass of electron, and ε_S and ε_0 are permittivity of ZnO NW and free space, respectively.[41] Figure 4b shows the extracted reverse-biased SBHs of ZnO NW device under different strains (from 0% to 0.96%). With V_G changing from −2 to 2 V, the SBH was decreased from 0.66 to 0.60 eV (at ε = 0.48%) due to the accumulation of free electrons in ZnO NW under positive V_G. From another point of view, under the same V_G (e.g., V_G = 0 V), the SBH decreased from 0.64 to 0.55 eV with the strain increasing from 0% to 0.96%. This was attributed to that more positive piezoelectric polarization charges were induced at the source-electrode/ZnO interface to attract more electrons under larger strain, resulting in corresponding current increment as shown in Figure 3a.

Based on the proposed theoretical model for piezotronic effect, the variation of the Schottky barrier heights ($\Delta\phi_b$) at M–S contact induced by the piezoelectric polarization charges is expressed as $\Delta\phi_b = -\frac{q^2\rho_{piezo}W_{piezo}^2}{2\kappa_{ZnO}}$, where q is the elementary charge, κ_{ZnO} is the dielectric constant of ZnO, ρ_{piezo} is the piezoelectric polarization charges density, and W_{piezo} is the distribution width of the polarization charges.[37,42] Taking into account the screening effect of electrons density (tuned by V_G through ion-gel) to the piezoelectric polarization charges (at M–S interface), the equation above can be modified as

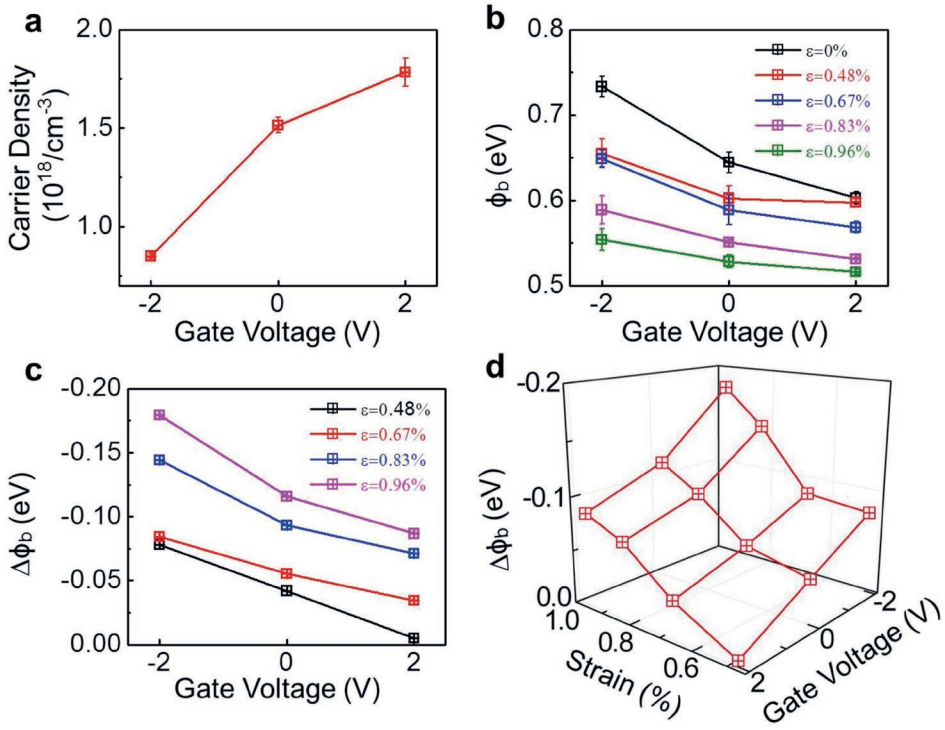

Figure 4. a) V_G dependence of carrier density in ZnO NWs. b) V_G dependence of reverse-bias SBHs under applied strains. c) V_G dependence of reverse-bias SBH variations under applied strains. d) SBH changes for different applied strains and V_Gs.

$$\Delta\phi_b = -\frac{q^2\left[a\left(\frac{1}{n}\right)^x + b\right]\rho_{piezo}W_{piezo}^2}{2\kappa_{ZnO}} = -\frac{q^2\rho_{effect}W_{piezo}^2}{2\kappa_{ZnO}} \quad (2)$$

Thereinto, $a\left(\frac{1}{n}\right)^x + b$ is the compensation factor to the effective piezoelectric polarization charges density (ρ_{effect}) determined by electrons density (n) modulated by V_G, where a, b, and x are the constant coefficients. Hence, the change in the SBH under different V_Gs can be used to speculate the influence of gate voltage on effective polarization charges. Notably, to simplify the ion-gel-gated M–S–M model, we mainly considered how the charge carrier density in the semiconductor NWs affected the piezotronic effect instead of the accumulated charges (or ions) at ion-gel/nanowire interface. More comprehensive theoretical studies are encouraged to add other compensation factors related with gate–semiconductor interface charges (or ions) to further evaluate SBH variation. To quantitatively evaluate the piezotronic effect, the variations of the reverse-biased SBH versus different ion-gel-gating voltages under different strains (from 0.48% to 0.96%) were calculated (Figure 4c). With ZnO NW subjection to certain strain, the variation of SBH at gate voltage of −2 V was larger than that under V_G at 0 or 2 V. This further demonstrated that the applied negative V_G could deplete the electrons density in ZnO NW, alleviated the screening effect on piezoelectric polarization charges and enhanced the piezotronic effect per unit strain. The SBH variation determined by the synergistic imposition of external strain and ion-gel-gating voltages is illustrated in Figure 4d. Ion-gel-gating at −2 V in coordination with applying tensile strain at 0.96% assumed the largest SBH modulation at 0.18 eV. The analysis of synergistic imposition on SBH variation is helpful to design high performance piezotronic devices.

Notably, the ion-gel was only patterned on a portion of the ZnO NW to avoid the risk of high leakage I_G from gate to Ag paste. The covered and uncovered parts of ZnO NW by ion-gel can be considered as homojunctions.[43] The corresponding discussion on the energy band structure is illustrated in Figure S8 (Supporting Information). To simply understand the modulation mechanism in this work, energy band diagrams of ZnO NWs under the synergistic imposition of external strains and different ion-gel-gating voltages were sketched in **Figure 5**. The black solid/dashed lines represent the initial band state of ZnO NW; the orange solid lines represent the band structure under applied gate voltage; the purple dashed lines represent the band structure change induced by applied strains; and the blue solid lines represent the final band structure of ZnO NW under both applied strain and gate voltage. Initially, a basic barrier (ϕ_0) formed at Ag–ZnO contact, as shown in Figure 5a. Before applying strains, the impact of gate voltage was illustrated first. In Figure 5b, a positive gate voltage was applied to induce the cations in ion-gel migrating to the surface of ZnO NW, leading to the accumulation of free electrons in ZnO and decreased SBH (ϕ_1), consistent with the slightly increased I_D in Figure 3b (compared with Figure 3a). Inversely, a negative gate voltage led to depletion of electrons and increased SBH (ϕ_2, Figure 5c), verified by the overall decrements of I_Ds in Figure 3c. The energy band diagram was further explained with applied strains. As shown in Figure 5d, the applied tensile strain (at V_G = 0) imposed the positive polarization charges distributed at the source-electrode/ZnO interface, leading to decreased reverse-biased SBH (ϕ_0'), with SBH variation at $\Delta\phi_0$. When the ZnO NW was imposed with both tensile strain and positive gate voltage (top panel in Figure 5e), the positive V_G increased the free electrons density and enhanced the screening effect to positive piezopolarization charges. The effective decreased piezocharges density led to the reverse-biased SBH decrement ($\Delta\phi_1$, induced by piezotronic effect) smaller than $\Delta\phi_0$ (i.e., weakening the piezotronic effect). The superimposition of tensile strain and positive V_G resulted in a smaller overall SBH (ϕ_1', $\phi_1' < \phi_1$ and $\phi_1' < \phi_0'$), consistent with the slightly increased I_Ds in Figure 3b. By contrast, when the ZnO NW was applied with tensile strain under negative gate voltage (Figure 5f), the depleted electrons density by negative V_G increased the effective piezocharges density (i.e., enhanced piezotronic effect), which enlarged the reverse-biased SBH decrement ($\Delta\phi_2$) with respect to SBH ($\Delta\phi_0$). However, the decreased electrons density by negative V_G dominated the transport properties of ZnO NW device, leading to a larger overall SBH (ϕ_2', $\phi_2' > \phi_0'$), consistent with the total decrement of I_Ds in Figure 3c. Notably, according to the contribution of enhanced piezotronic effect which increased the output current, we could speculate that overall SBH in Figure 5f was smaller than that in Figure 5c, i.e., $\phi_2' < \phi_2$. If the ZnO NW device was subjected to the compressive stain (top panel in Figure 5g), negative polarization charges were accumulated at the reverse-biased Schottky contact, which inhibited the electrons transport in ZnO and led to an increased SBH (bottom panel in Figure 5g). When the positive V_G was applied to the compressive ZnO NW device, the electrons density was increased in the ZnO NW channel. Thus, more electrons were able to be tuned by the negative polarization charges, equivalent to an enhanced piezotronic effect ($\Delta\phi_1' > \Delta\phi_0'$, Figure 5h). On the contrary, negative V_G depleted the electrons in ZnO NW, less electrons were available to be controlled by the negative polarization charges, exhibiting a weakened piezotronic effect ($\Delta\phi_2' < \Delta\phi_0'$, Figure 5i). The variation process of the energy band diagrams of ZnO NW device is illustrated in Figure S9 (Supporting Information) in detail.

All the results above demonstrate that the ion-gel-gating modulation can effectively modulate the piezotronic effect, which has great potential in highly sensitive piezotronic strain sensor and tunable logic devices. The piezotronic device itself can work as a strain sensor. The strain dependent output currents of ion-gel-gated piezotronic strain sensor under different V_Gs are shown in **Figure 6**a. The gauge factor (GF) is defined as $(\Delta I_\varepsilon/I_0)/\varepsilon$ (thereinto, ΔI_ε is the current variation under external strain, and I_0 is output current without strain).[44] To verify the ion-gel-gating effect on the sensitivity of the strain sensor, Figure 6b shows GF versus external strain under different V_Gs. For a certain tensile strain, the gauge factor under gating modulation at −2 V is obviously greater than the gating situation under 0 and 2 V. It indicated that the sensitivity of the piezotronic strain sensor could be efficiently modulated through ion-gel-gating. A piezotronics logic device is fabricated by connecting an ion-gel-gated ZnO NW device in series with a 10 MΩ resistor (Figure 6c). The voltage transfer characteristic of the piezotronics logic device is

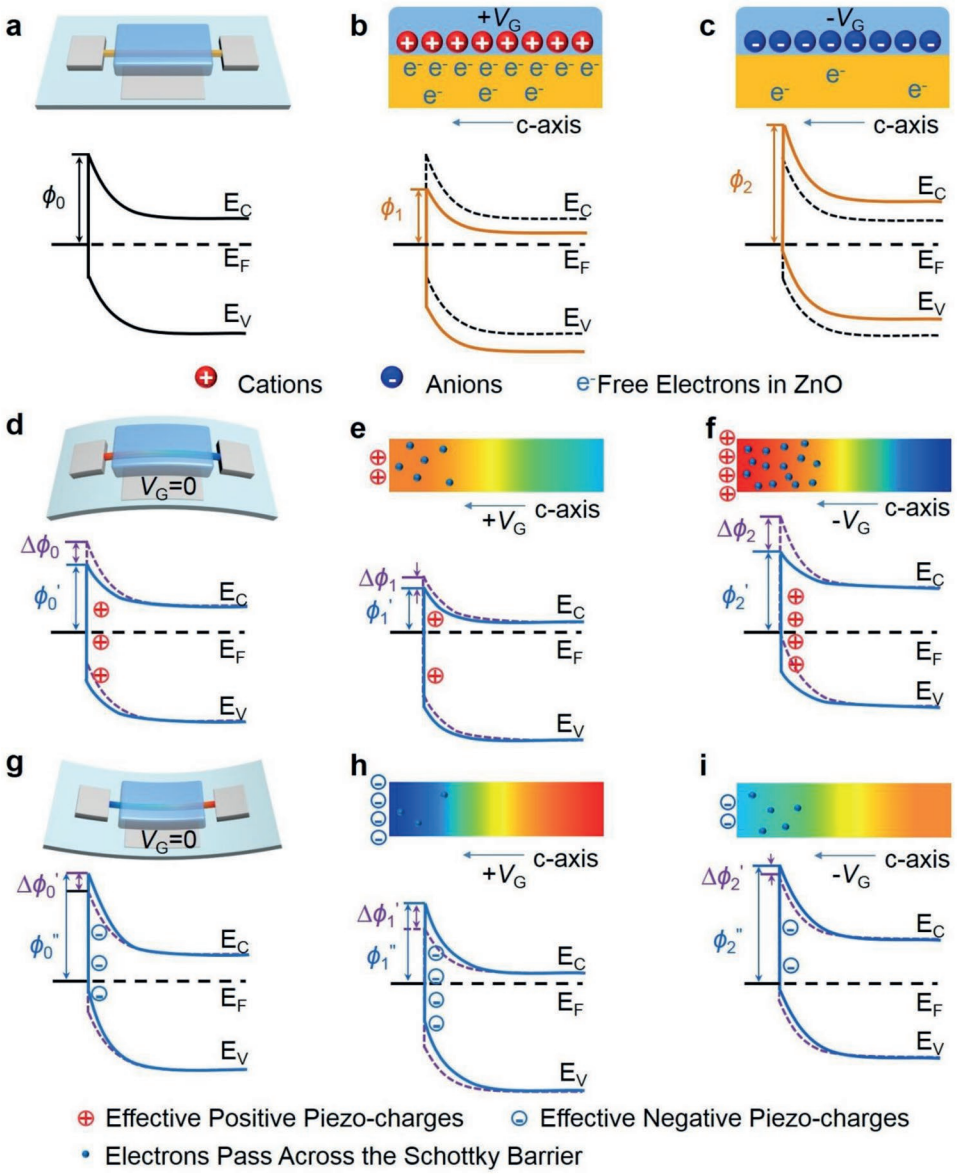

Figure 5. The modulation mechanism of ion-gel channel-width gating on piezotronics interface gating in ZnO NW. a) Without strain and gate voltage; b) with positive V_G; c) with negative V_G; d) with applied tensile strain; e) with applied tensile strain and positive V_G; f) with applied tensile strain and negative V_G; g) with applied compressive strain; h) with applied compressive strain and positive V_G; i) with applied compressive strain and negative V_G.

shown in Figure 6d. The logic separation (variation of the output voltage, V_{OUT}) under ion-gel-gating at −2 V is larger than the positive and zero-bias gating situations. Figure 6e showed the real-time output characteristics of the logic device by periodically applying/releasing 0.96% strain on ZnO NW at different V_Gs (V_G = 0, 2, and −2 V). When a 0.96% tensile strain was applied to the device, V_{OUT} increased from 1.30 to 1.70 V under no gate bias. By contrast, V_{OUT} increased from 1.46 to 1.72 V under V_G at 2 V, and increased from 0.69 to 1.48 V under V_G at −2 V. The variations of the V_{OUT} under external strain of 0.96% at different V_Gs were displayed in Figure 6f. Ion-gel-gating at −2 V resulted in the largest modulation (0.79 V) on the V_{OUT}, increased by 97.5%. The demonstrated enhancement in GF and tunability in piezotronic devices are attributed to the modulation of piezotronic effect by ion-gel-gating. The solid-state electrolyte method enables highly efficient modulation on piezotronic effect, offering a new way to realizing low-power consuming and sophisticated piezotronic devices.

3. Conclusions

In summary, a highly efficient and low-energy-consuming way to modulate the piezotronic interface gating through ion-gel channel-width gating was demonstrated in this work. The ultrahigh capacitance of ion-gel resulting from EDLs enabled efficient modulation of electrons density in ZnO NW at ultralow gate voltage (2 V). Negative gate voltage could deplete free electons

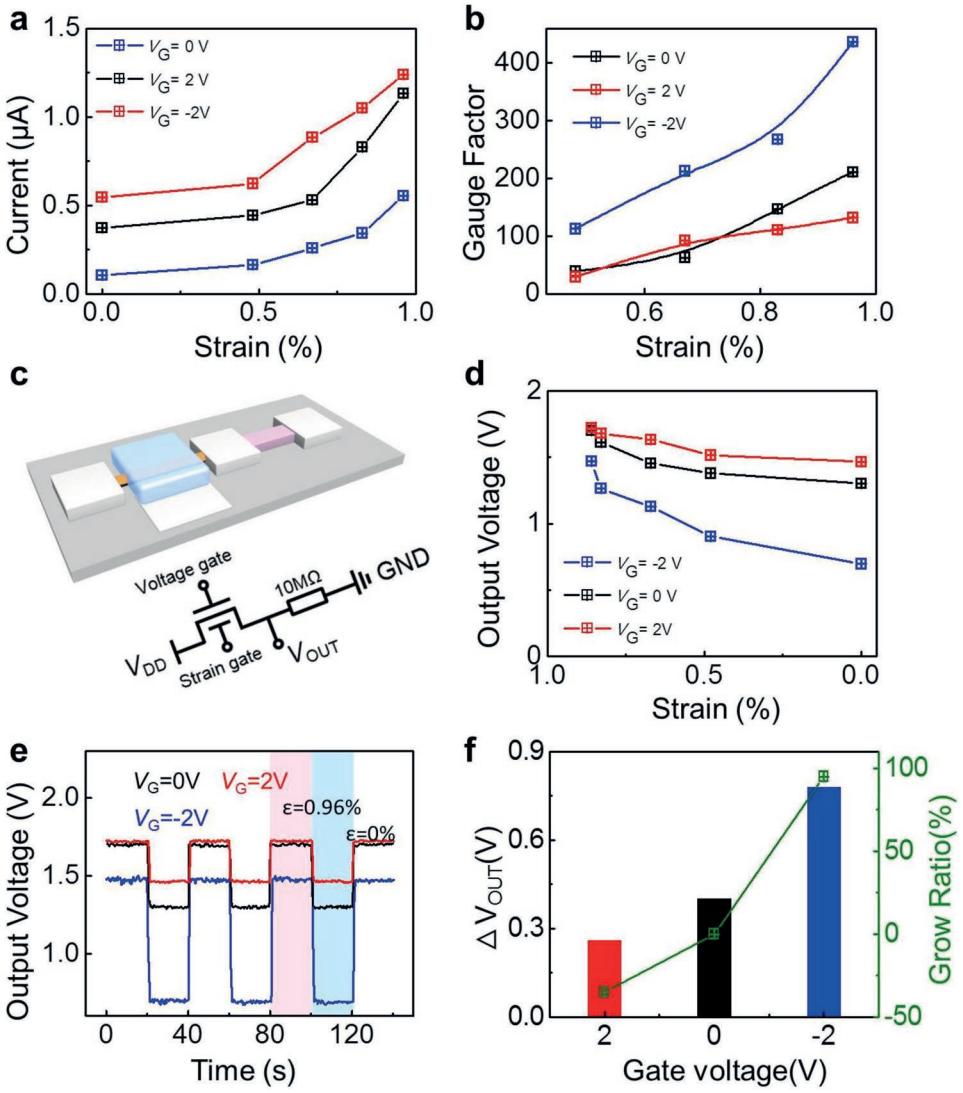

Figure 6. Application of ion-gel-gated piezotronic ZnO NWs. a) Current versus strains under different V_G at V_D = 2 V for the ZnO NWs based strain sensor. b) Gauge factor versus strain under different V_G for the ZnO NWs based pressure sensor. c) Schematic diagram of a tunable piezotronic logic device, an ion-gel-gated ZnO NW device connecting in series with a 10 MΩ resistance. d) Voltage transfer characteristic of the piezotronic logic device. e) Real time *V*–*t* characteristics of the logic device by applying/removing a 0.96% strain periodically on ZnO NWs under different gate voltage (V_G = 0 V, V_G = 2 V, and V_G = −2 V) at V_{DD} = 2 V. f) The change of output voltage (ΔV_{out}) under different V_Gs and the corresponding change ratios related to the condition without gate voltage.

in ZnO to weaken the screening effect on positive polarization charges, realizing an enhanced piezotronic response. The working mechanism was theoretically supported by a calculation of Schottky barrier height through the M–S–M model. Through ion-gel gating, applied negative gate voltage was also capable of improving the gauge factor of a piezotronic sensor and the output properties of a piezoelectric inverter. The ion-gel-gating method offers a solid-state, efficient, low power, and universal way to modulate piezotronic transistors, sensors, and logic devices, which has great potential in piezotronic computation, high performance wearable sensors, high resolution E-skin, and tunable piezophototronic devices.

According to the large specific capacitance, excellent mechanical properties, high ionic conductivity, and printability, ion-gel has been widely used as the gate dielectrics in transistor to realize low-voltage operation[45] and highly stretchable electronic devices.[46,47] According to the liquid to gel transition during processing, the ion-gel can fully contact with the target nano-semiconductors (e.g., fill in the charge traps in colloidal nanocrystals[48] and surround the nanowires[43]) to realize high performance gating properties. Moreover, the induced charge carrier density and high capacitance of ion-gel are hardly affected by the external strains, which are ready to achieve stable flexible/stretchable devices and allow authentic investigation on the strain-controlled charge transport properties. Taking advantage of all the benefits in ion-gel, the EDL gating assumes an efficient way to the investigation of solid-state fundamental physical phenomena, low cost and ultralow power consuming electronic devices, highly interactive artificial sensing, intelligence and soft robotics, etc.

4. Experimental section

The Synthesis of ZnO NWs: The ZnO NWs used in this work were synthesized via a vapor trapping CVD method. ZnO powder and graphite powder, as source materials, were dispersed in ethanol in the weight ratio of 1:1. The mixture was ground incessantly for 5–6 h, and then dried in an oven at 70 °C for 3h. The preprocessed source materials were transferred into an alumina boat, with target silicon wafer substrates covered on the boat with polished surface facing down. The whole set was located at the center of a quartz tube furnace, heated at 960 °C for 30 min with a constant flow of carries gas (30 sccm of argon and 10 sccm of oxygen).

The Fabrication and Characterization of the ZnO NWs Device: First, the PET substrate (1 cm × 3 cm, 0.5 mm in thickness) was cleaned with alcohol, isopropyl, and deionized water by sonication. Second, the photoresist (AZ 5214E) was spin-coated on this substrate. After baking at 90 °C for 45 s to remove the solvent, the photoresist was patterned by UV-lithography (MA6, Karl Suss). Then Cr/Ag film (5/30 nm) was thermally deposited on it, followed by a lift-off progress to define the gate, drain, and source electrodes. Next, the selected ZnO NW was picked up under the coordination of a syringe needle (vacuum adsorption) and a tweezer with sharp tip (tip diameter is 0.06 mm) and located between the source and drain electrodes assisted with an optical microscope. Then the ion-gel was precisely patterned across the ZnO NWs and a portion of the gate electrode. Finally, silver paste was dropped on two ends of the ZnO NW to fix it. All the *I–V* transistor characteristics of the device under different applied strains and gate voltages were obtained at room temperature under ambient conditions using a Semiconductor Device Analyzer (1500A, Keysight, America).

The Impedance Analysis of the Ion Gel: Capacitance measurements were carried out using an electrical work station (CHI 660E) at room temperature. Au electrodes with channel length at 50 µm were first patterned on a Si wafer, and then the ion-gel was patterned across them, having a 0.5 cm^2 contact area with two electrodes, respectively. The measurement was conducted over the frequency range of 0.1–10^5 Hz with AC amplitude of 10 mV.

Supporting Information

Supporting Information is available from the Wiley Online Library or from the author.

Acknowledgements

X.Y. and G.H. contributed equally to this work. This work was financially supported by the National Key Research and Development Program of China (Grant Nos. 2016YFA0202703 and 2016YFA0202704), the National Natural Science Foundation of China (Grant Nos. 51605034, 51711540300, and 51475099), the "Hundred Talents Program" of the Chinese Academy of Science and State key laboratory of precision measuring technology and instruments (Tianjin University).

Conflict of Interest

The authors declare no conflict of interest.

Keywords

coupling, electric double layer, ion-gel gating, piezotronic effect, ZnO nanowire

Received: November 5, 2018
Revised: December 13, 2018
Published online: February 6, 2019

[1] Z. L. Wang, J. H. Song, *Science* **2006**, *312*, 242.
[2] Z. L. Wang, *Nano Today* **2010**, *5*, 540.
[3] X. Wang, R. Yu, C. Jiang, W. Hu, W. Wu, Y. Ding, W. Peng, S. Li, Z. L. Wang, *Adv. Mater.* **2016**, *28*, 7234.
[4] W. Wu, L. Wang, Y. Li, F. Zhang, L. Lin, S. Niu, D. Chenet, X. Zhang, Y. Hao, T. F. Heinz, J. Hone, Z. L. Wang, *Nature* **2014**, *514*, 470.
[5] W. Wu, X. Wen, Z. L. Wang, *Science* **2013**, *340*, 952.
[6] J. Zhou, P. Fei, Y. F. Gao, Y. D. Gu, J. Liu, G. Bao, Z. L. Wang, *Nano Lett.* **2008**, *8*, 2725.
[7] S. Liu, Q. Liao, S. Lu, Z. Zhang, G. Zhang, Y. Zhang, *Adv. Funct. Mater.* **2016**, *26*, 1347.
[8] J. Shi, M. B. Starr, H. Xiang, Y. Hara, M. A. Anderson, J. H. Seo, Z. Ma, X. Wang, *Nano Lett.* **2011**, *11*, 5587.
[9] R. Yu, C. Pan, J. Chen, G. Zhu, Z. L. Wang, *Adv. Funct. Mater.* **2013**, *23*, 5868.
[10] C. Pan, R. Yu, S. Niu, G. Zhu, Z. L. Wang, *ACS Nano* **2013**, *7*, 1803.
[11] J. Zhou, P. Fei, Y. D. Gu, W. J. Mai, Y. F. Gao, R. S. Yang, G. Bao, Z. L. Wang, *Nano Lett.* **2008**, *8*, 3973.
[12] W. Wu, Z. L. Wang, *Nano Lett.* **2011**, *11*, 2779.
[13] W. Wu, Y. Wei, Z. L. Wang, *Adv. Mater.* **2010**, *22*, 4711.
[14] R. Yu, W. Wu, C. Pan, Z. Wang, Y. Ding, Z. L. Wang, *Adv. Mater.* **2015**, *27*, 940.
[15] X. Han, W. Du, M. Chen, X. Wang, X. Zhang, X. Li, J. Li, Z. Peng, C. Pan, Z. L. Wang, *Adv. Mater.* **2017**, *29*, 1701253.
[16] C. Pan, L. Dong, G. Zhu, S. Niu, R. Yu, Q. Yang, Y. Liu, Z. L. Wang, *Nat. Photonics* **2013**, *7*, 752.
[17] Y. Hu, B. D. Klein, Y. Su, S. Niu, Y. Liu, Z. L. Wang, *Nano Lett.* **2013**, *13*, 5026.
[18] G. Hu, R. Zhou, R. Yu, L. Dong, C. Pan, Z. L. Wang, *Nano Res.* **2014**, *7*, 1083.
[19] F. Xue, L. Zhang, X. Feng, G. Hu, F. R. Fan, X. Wen, L. Zheng, Z.L. Wang, *Nano Res.* **2015**, *8*, 2390.
[20] D. Zhou, R. Liu, J. Zhang, X. Qi, Y. He, B. Li, Q. Yang, Y. Hu, F. Kang, *Nano Energy* **2017**, *33*, 45.
[21] S. Qin, Q. Zhang, X. Yang, M. Liu, Q. Sun, Z. L. Wang, *Adv. Energy Mater.* **2018**, *8*, 1800069.
[22] H. C. Moon, C. H. Kim, T. P. Lodge, C. D. Frisbie, *ACS Appl. Mater. Interfaces* **2016**, *8*, 6252.
[23] Q. Zhao, J. Heyda, J. Dzubiella, K. Tauber, J. W. Dunlop, J. Yuan, *Adv. Mater.* **2015**, *27*, 2913.
[24] Q. Sun, D. H. Kim, S. S. Park, N. Y. Lee, Y. Zhang, J. H. Lee, K. Cho, J. H. Cho, *Adv. Mater.* **2014**, *26*, 4735.
[25] H. Yuan, H. Shimotani, A. Tsukazaki, A. Ohtomo, M. Kawasaki, Y. Iwasa, *Adv. Funct. Mater.* **2009**, *19*, 1046.
[26] G. Zhu, Y. Zhou, S. Wang, R. Yang, Y. Ding, X. Wang, Y. Bando, Z. Wang, *Nanotechnology* **2012**, *23*, 055604.
[27] R. Liu, X. C. You, X. W. Fu, F. Lin, J. Meng, D. P. Yu, Z. M. Liao, *Sci. Rep.* **2015**, *5*, 10125.
[28] B. Nie, J. G. Hu, L. B. Luo, C. Xie, L. H. Zeng, P. Lv, F. Z. Li, J. S. Jie, M. Feng, C. Y. Wu, Y. Q. Yu, S. H. Yu, *Small* **2013**, *9*, 2872.
[29] S. Z. Bisri, S. Shimizu, M. Nakano, Y. Iwasa, *Adv. Mater.* **2017**, *29*, 1607054.
[30] D. Braga, I. Gutierrez Lezama, H. Berger, A. F. Morpurgo, *Nano Lett.* **2012**, *12*, 5218.
[31] J. K. Huang, J. Pu, C. L. Hsu, M. H. Chiu, Z. Y. Juang, Y. H. Chang, W. H. Chang, Y. Iwasa, T. Takenobu, L. J. Li, *ACS Nano* **2014**, *8*, 923.
[32] K. H. Lee, M. S. Kang, S. Zhang, Y. Gu, T. P. Lodge, C. D. Frisbie, *Adv. Mater.* **2012**, *24*, 457.
[33] S. H. Kim, K. Hong, W. Xie, K. H. Lee, S. Zhang, T. P. Lodge, C. D. Frisbie, *Adv. Mater.* **2013**, *25*, 1822.
[34] W. Xie, C. D. Frisbie, *J. Phys. Chem. C* **2011**, *115*, 14360.
[35] M. S. Kang, J. Lee, D. J. Norris, C. D. Frisbie, *Nano Lett.* **2009**, *9*, 3848.

[36] Q. Zhang, T. Jiang, D. Ho, S. Qin, X. Yang, J. H. Cho, Q. Sun, Z. L. Wang, *ACS Nano* **2018**, *12*, 254.
[37] J.-H. Lee, K. Y. Lee, B. Kumar, N. T. Tien, N.-E. Lee, S.-W. Kim, *Energy Environ. Sci.* **2013**, *6*, 169.
[38] Z. Pan, W. Peng, F. Li, Y. He, *Nano Energy* **2018**, *49*, 529.
[39] Z. Zhang, K. Yao, Y. Liu, C. Jin, X. Liang, Q. Chen, L. M. Peng, *Adv. Funct. Mater.* **2007**, *17*, 2478.
[40] Y. Liu, Z. Y. Zhang, Y. F. Hu, C. H. Jin, L. M. Peng, *J. Nanosci. Nanotechnol.* **2008**, *8*, 252.
[41] Y. Zhang, Y. Liu, Z. L. Wang, *Adv. Mater.* **2011**, *23*, 3004.
[42] J. Shi, M. B. Starr, X. Wang, *Adv. Mater.* **2012**, *24*, 4683.
[43] A. M. Burke, D. J. Carrad, J. G. Gluschke, K. Storm, S. Fahlvik Svensson, H. Linke, L. Samuelson, A. P. Micolich, *Nano Lett.* **2015**, *15*, 2836.
[44] Y. Liu, M. Z. Kauser, D. D. Schroepfer, P. P. Ruden, J. Xie, Y. T. Moon, N. Onojima, H. Morkoç, K. A. Son, M. I. Nathan, *J. Appl. Phys.* **2006**, *99*, 113706.
[45] K. Hong, S. H. Kim, K. H. Lee, C. D. Frisbie, *Adv. Mater.* **2013**, *25*, 3413.
[46] S. K. Lee, B. J. Kim, H. Jang, S. C. Yoon, C. Lee, B. H. Hong, J. A. Rogers, J. H. Cho, J. H. Ahn, *Nano Lett.* **2011**, *11*, 4642.
[47] F. Xu, M. Y. Wu, N. S. Safron, S. S. Roy, R. M. Jacobberger, D. J. Bindl, J. H. Seo, T. H. Chang, Z. Ma, M. S. Arnold, *Nano Lett.* **2014**, *14*, 682.
[48] M. I. Nugraha, H. Matsui, S. Watanabe, T. Kubo, S. Z. Bisri, H. Roger, M. Sytnyk, W. Heiss, M. A. Loi, J. Takeya, *Adv. Electron. Mater.* **2017**, *3*, 1600360.